DNS of a Periodic Channel Flow with Isothermal Ablative Wall

Olivier Cabrit, Franck Nicoud

DNS of a periodic channel flow with isothermal ablative wall

O. Cabrit[1] and F. Nicoud[2]

[1] CERFACS, 42 avenue Gaspard Coriolis, 31057 Toulouse, France
olivier.cabrit@cerfacs.fr
[2] Université Montpellier 2, Place Eugène Bataillon, 34095 Montpellier, France
franck.nicoud@univ-montp2.fr

1 Introduction

Ablative surface flows often arise when using thermal protection materials for preserving structural component of atmospheric re-entry spacecrafts[1] and Solid Rocket Motors (SRM) internal insulation or nozzle assembly[2]. In the latter application, carbon-carbon composites are widely used and exposed to severe thermochemical attack. The nozzle surface recedes due to the action of oxidizing species, typically H_2O and CO_2, which is an issue during motor firing since the SRM performance is lowered by the throat area increase and the apparition of surface roughness. Full-scale motor firings are very expensive and do not provide sufficient information to understand the whole phenomenon. Numerical simulations can then be used to generate precise and detailed data set of generic turbulent flows under realistic operating conditions.

Many studies have already proposed to couple numerically the gaseous phase and the solid structure[3, 4, 5]. However, most of them are dedicated to the structural material characterization by predicting the recession rate or the surface temperature and few are dealing with the fluid characterization. Hence, the objective of the present study is to increase the understanding of changes of the turbulent boundary layer (TBL) when thermochemical ablation occurs. In this framework, the present study aims at presenting the results obtained from a DNS of turbulent reacting multicomponent channel flow with isothermal ablative walls. Another simulation led under the same operating conditions but with inert walls will constitute a reference case. Results of the preliminary study[6] have been improved thanks to an ensemble average procedure giving more details on mass/momentum/energy conservations.

The full 3D compressible reacting Navier-Stokes equations are solved by using the AVBP code developed at CERFACS. This third-order accurate solver (in both space and time) is dedicated to LES/DNS of reacting flows and has been widely used and validated during the past years[7, 8].

The classical channel flow configuration[9] is used in this study. As shown in Fig. 1, periodic boundary conditions are used in both streamwise and spanwise directions. A no-slip isothermal boundary condition is imposed for inert case while a blowing isothermal boundary condition is set for the ablation case (see below for its description). Moreover, the streamwise flow is enforced by adding a source term to the momentum conservation equation while a volume source term that warms the fluid is added to the energy conservation equation in order to sustain the mean temperature inside the computational domain.

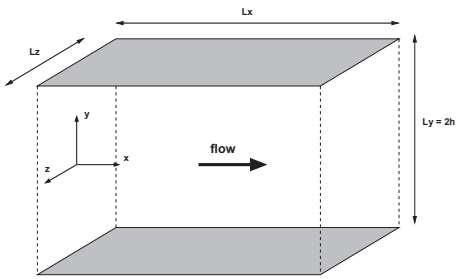

DNS	Re_τ	Lx/h	Lz/h	wall B.C.
Inert	300	3.2	1.25	isothermal/no-slip
	homogeneous directions: x, z, t			
ablation	300	3.2	1.25	isothermal/blowing
	homogeneous directions: x, z			

Fig. 1. Computational domain.

Realistic gas ejected from SRM nozzles contains about a hundred gaseous species. Only the ones whose mole fraction is greater than 0.001 are kept to generate a simpler mixture, nitrogen being used as a dilutent. Hence, seven species are kept for the simulation: H_2, H, H_2O, OH, CO_2, CO and N_2. To simulate the chemical kinetics of this mixture, one applies a kinetic scheme based on seven chemical reactions extracted from the GRI-Mech elementary equations (see http://www.me.berkeley.edu/gri_mech).

For simplification reasons, the questions of two-phase flow effects, mechanical erosion and surface roughness will not be discussed in the present work. Hence, inspired by the wall recession model proposed by Keswani and Kuo[3] and the work of Kendall, Rindal and Bartlett[5] a reacting gaseous phase model is merely coupled with a boundary condition for thermochemically ablated walls. A full description of the boundary condition is given in Ref. [6]. It is based on the mass budget of the species k at the solid surface:

$$\rho_w Y_{k,w} \left(V_{inj} + V_k\right) = \dot{s}_k \tag{1}$$

where subscript w refers to wall quantities, ρ_w denotes the density of the mixture, $Y_{k,w}$ the mass fraction of species k, V_{inj} the convective velocity of the mixture at the surface, V_k the diffusion velocity of k in the direction normal to the wall and $\dot{s}_k$ the production rate of k. One obtains the injection velocity (also called Stephan velocity) by summing over all the species:

$$V_{inj} = \frac{1}{\rho_w} \sum_k \dot{s}_k \tag{2}$$

Moreover, making use of the Hirschfelder and Curtiss approximation with correction velocity for diffusion velocities[10], it is possible to relate $Y_{k,w}$ to its normal gradient at the solid/gas interface:

$$-\mathcal{D}_k \nabla Y_{k,w} + Y_{k,w} \left(V_{inj} + V^{cor} + W_w \mathcal{D}_k \sum_i \frac{\nabla Y_{i,w}}{W_i} \right) = \frac{\dot{s}_k}{\rho_w} \tag{3}$$

where $\mathcal{D}_k$ is the diffusion coefficient of k in the mixture, W_k the molecular weight of k, W_w the mean molecular weight of the mixture at the wall, $X_{k,w}$ the mole fraction of k and V^{cor} a correction diffusion velocity that ensures global mass conservation. The latter equation is used as a boundary condition for species k while (2) is used for the normal momentum equation. Note that because the production rate of species k depends on the concentration of the oxidizing species at the wall surface, the Stephan velocity is both space and time dependent which differs from the classical blowing surface DNS[11].

One single chemical reaction is accounted for at the interface, namely $C + H_20 \rightarrow H_2 + CO$. However, more complex oxidation schemes can be used within the framework described above.

2 Results

The DNS with ablative walls is statistically unsteady because the oxidation reaction at the wall consumes the H_2O species initially present in the computational domain. Thus, the data cannot be averaged over time which makes harder the statistics convergence (the computational box size should be about a hundred times wider to obtain converged statistics at a given time). Moreover, the time advancement of the DNS is dependent on the initial condition. For these reasons, to look at relevant data we have performed an ensemble average from twenty different DNS's with ablative walls, differing because of the initial conditions. To insure time decorrelation, the initial conditions are chosen from the inert wall simulation with a separating time taken to the diffusion time, $\tau_d = h/\sqrt{\overline{\tau_w}/\overline{\rho_w}}$. The statistics convergence with this procedure is illustrated by Figure 2.

Another question now arises: how do one has to look at into the generated data to observe a representative behavior of a generic TBL with wall ablation?

Indeed, the main difference between the simulated and the real cases is that the oxidizing species are continuously consumed in the simulated case (which means that no ablation would be observed for an infinite simulated time) whereas in the real case the combustion products passing through the nozzle continuously bring oxidizing species. This implies to find the appropriate scalings of the different observed variables to render them time independent. For instance, Figure 2-b) illustrates that the statistics cannot be performed before $\tau_s = \tau_d$ which is the necessary time for the flow to adapt from the inert wall initial condition. For $\tau_s > \tau_d$, the oxidation mechanisms is mainly led by the diffusion of oxidizing species towards the wall and unsteady terms tend to constant values which facilitates the research of a time-autosimilar behavior of the TBL. Figure 3 shows that a proper scaling is found by normalizing the atomic mole fraction profiles by their centerline value. Looking at Fig. 3-b) it is clear that the profiles do not collapse for $\tau_s < \tau_d$. This plot also illustrates the significant changes of atomic composition arising inside the ablative wall TBL which explains that contrary to the inert wall case the equilibrium state is not only dependent on the temperature profile when ablation occurs[6]. This is presented in Fig. 4 for the oxidizing species H_2O. The presented results are also worthwhile for other atoms and species but not shown herein.

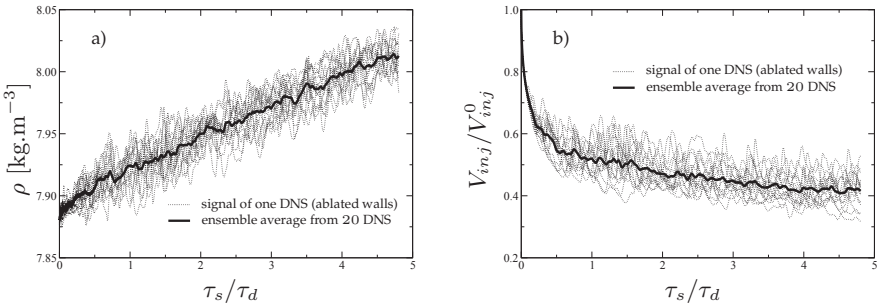

Fig. 2. Evolution of the density (a) and of the injection velocity (b) for one probe situated at the wall during the ablative wall simulation. The velocity is scaled by the initial injection velocity, V^0_{inj}, and the simulated time, τ_s, is scaled by τ_d.

For the present channel flow configuration, the specific enthalpy conservation equation can be written as:

$$\frac{d}{dy}\underbrace{\left(q_{h_s} + q_{h_c} + q_{Fourier} + q_{spec}\right)}_{q_{tot}} = \overline{\mathcal{Q}} \tag{4}$$

where q_{h_s} is the heat flux of sensible enthalpy, q_{h_c} the heat flux of chemical enthalpy, $q_{Fourier}$ the Fourier heat flux, q_{spec} the heat flux of species diffusion, and $\overline{\mathcal{Q}}$ the enthalpy source term that warms the fluid to sustain the mean temperature. Figure 5 presents each term of the total heat flux balance for

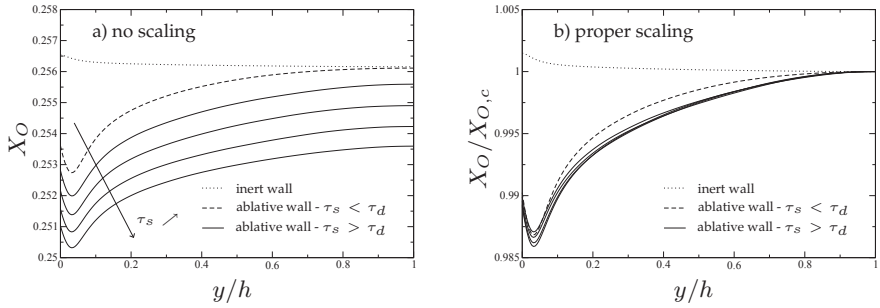

Fig. 3. Atomic mole fraction profiles of O: a) without scaling; b) scaled by its centerline value $X_{O,c}$.

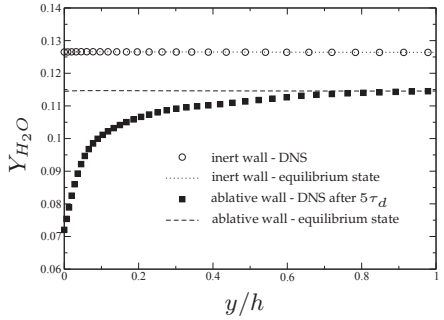

Fig. 4. Mass fraction profiles of H_2O: comparison between the DNS and the chemical equilibrium state assessed from the CHEMKIN software using the mixture composition at $y = h$ and the DNS temperature profile.

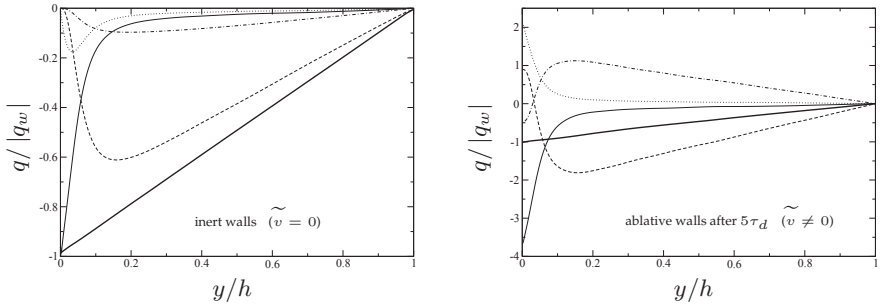

Fig. 5. Heat flux balance scaled by the modulus of the flux at the wall $|q_w|$. - - - - : flux of sensible enthalpy, $q_{h_s} = \overline{\rho}\,(\widetilde{v''h''_s} + \widetilde{v}\widetilde{h}_s)$; — · — : flux of chemical enthalpy, $q_{h_c} = \overline{\rho}\,\sum_k(\widetilde{v''Y''_k} + \widetilde{v}\widetilde{Y}_k)\Delta h^0_{f,k}$; ——— : Fourier heat flux, $q_{Fourier} = -\overline{\lambda\frac{dT}{dy}}$; ····· : species diffusion flux, $q_{spec} = \overline{\rho}\sum_k\{h_kY_kV_{k,y}\}$, ($\{h_kY_kV_{k,y}\}$ is a Favre average quantity); ——— : full total heat flux, q_{tot}.

the inert wall case and the ablation one after $\tau_s = 5\tau_d$. One first see that according to the specific enthalpy balance, Eq.(4), the total heat flux is linear through the boundary layer in both cases, the slope being related to the source term $\overline{\mathcal{Q}}$ which is constant in space. However, strong differences are visible, notably because of the blowing effect of the ablation process. Indeed, for inert walls the no-slip boundary condition at the wall combined with the continuity equation imposes that $\widetilde{v} = 0$ ($\widetilde{v}$ being the Favre average wall normal velocity). This is not the case for ablative wall DNS. In addition, the diffusion velocities are not null at the ablative wall. As a consequence, none of the terms of the heat flux balance are null (neither negligible) at the ablative wall whereas the total heat flux is recovered by the Fourier heat flux at the inert wall. This is emphasized by Fig. 6 that shows the time evolution of the different heat fluxes at the wall during the ablative wall simulation. This figure shows that the heat fluxes of sensible enthalpy and of species diffusion are responsible for surface cooling which explains that the total wall heat flux is lowered by a factor 3.5 in the ablative wall DNS compared to the inert one. Moreover, this plot shows that the scaling of the heat flux by the total wall heat flux modulus converges after $\tau_s = 4\tau_d$. This result justifies that observing the data at $\tau_s = 5\tau_d$ (as in Fig. 5) gives a representative state of the ablative wall TBL.

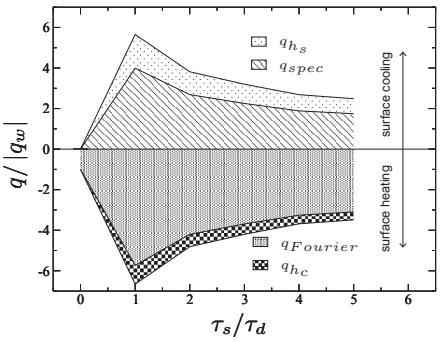

Fig. 6. Time evolution of the heat fluxes at the wall during the ablative wall simulation.

Concerning the momentum conservation balance, the wall ablation makes appear a convective term, namely $-\overline{\rho}\ \widetilde{u}\ \widetilde{v}$. However, the mass flux ratio, $F = \overline{\rho_w\ V_{inj}}/\rho_b u_b$ (b-subscripted variables refer to bulk value), of the current simulation is too weak to change the shear stress balance. Indeed, $F \approx 0.02\%$ in the DNS which is very low compared to the values found in classical blowing surface studies[12]. This convective term is thus negligible, leading to the same shear stress conservation mechanism for both inert and ablative wall TBL.

3 Conclusion

This study brings some keys in performing a DNS of periodic channel flow with ablative walls. It is shown that with the framework describes above, the generated data cannot be analyzed for $\tau_s < \tau_d$ and that the time dependency could be cut off by using appropriate scalings. In this way it is possible to analyze the behavior of a generic ablative wall TBL. The analysis of the shear stress and heat flux balances reveals the negligible terms and explains the surface cooling effect of wall ablation.

References

1. J. Zhong, T. Ozawa, and D. A. Levin. Modeling of stardust reentry ablation flows in near-continuum flight regime. A*IAA J.*, 46(10):2568–2581, October 2008.
2. J. H. Koo, D. W. H. Ho, and O. A. Ezekoye. A review of numerical and experimental characterization of thermal protection materials - part I. numerical modeling. In *42nd AIAA/ASME/SAE/ASEE Joint Propulsion Conference and Exhibit*, Sacramento, California, 9-12 July 2006.
3. S. T. Keswani and K. K. Kuo. An aerothermochemical model of carbon-carbon composite nozzle recession. *AIAA Paper 83-910*, 1983.
4. P. Baiocco and P. Bellomi. A coupled thermo-ablative and fluid dynamic analysis for numerical application to solid propellant rockets. *AIAA Paper 96-1811*, June 1996.
5. R. M. Kendall, R. A. Rindal, and E. P. Bartlett. A multicomponent boundary layer chemically coupled to an ablating surface. *AIAA Journal*, 5(6):1063–1071, 1967.
6. O. Cabrit, L. Artal, and F. Nicoud. Direct numerical simulation of turbulent multispecies channel flow with wall ablation. *AIAA Paper 2007-4401*, 39th AIAA Thermophysics Conference, June 2007.
7. P. Schmitt, T. J. Poinsot, B. Schuermans, and K. Geigle. Large-eddy simulation and experimental study of heat transfer, nitric oxide emissions and combustion instability in a swirled turbulent high pressure burner. J. *Fluid Mech.*, 570:17–46, 2007.
8. S. Mendez and F. Nicoud. Large-eddy simulation of a bi-periodic turbulent flow with effusion. J. *Fluid Mech.*, 598:27–65, 2008.
9. J. Kim, P. Moin, and R. Moser. Turbulence statistics in fully developed channel flow at low Reynolds number. J. *Fluid Mech.*, 177:133–166, 1987.
10. J.O. Hirschfelder, F. Curtiss, and R.B. Bird. *Molecular theory of gases and liquids*. John Wiley & Sons, 1964.
11. Y. Sumitani and N. Kasagi. Direct numerical simulation of turbulent transport with uniform wall injection and suction. A*IAA J.*, 33(7):1220–1228, July 1995.
12. R. L. Simpson. Characteristics of turbulent boundary layers at low Reynolds numbers with and without transpiration. J. *Fluid Mech.*, 42(4):769–802, 1970.